

# Few-Mode-Fiber Technology Fine-tunes Losses in Quantum Communication Systems

A. Alarcón<sup>1</sup>, J. Argillander<sup>1</sup>, G. Lima,<sup>2,3</sup> and G.B. Xavier<sup>1,\*</sup>

<sup>1</sup>*Institutionen för Systemteknik, Linköpings Universitet, SE-581 83 Linköping, Sweden*

<sup>2</sup>*Departamento de Física, Universidad de Concepción, Casilla 160-C, Concepción, Chile*

<sup>3</sup>*Millennium Institute for Research in Optics, Universidad de Concepción, Casilla 160-C, Concepción, Chile*

(Received 1 April 2021; revised 9 August 2021; accepted 10 August 2021; published 9 September 2021; corrected 4 October 2021 and 2 December 2022)

A natural choice for quantum communication is to use the relative phase between two paths of a single photon for information encoding. This method was nevertheless quickly identified as impractical over long distances, and thus a modification based on single-photon time bins has become widely adopted. It, however, introduces a fundamental loss, which increases with the dimension and limits its application over long distances. Here solve this long-standing hurdle by using a few-mode-fiber space-division-multiplexing platform working with orbital-angular-momentum modes. In our scheme, we maintain the practicability provided by the time-bin scheme, while the quantum states are transmitted through a few-mode fiber in a configuration that does not introduce postselection losses. We experimentally demonstrate our proposal by successfully transmitting phase-encoded single-photon states for quantum cryptography over 500 m of few-mode fiber, showing the feasibility of our scheme.

DOI: 10.1103/PhysRevApplied.16.034018

## I. INTRODUCTION

Quantum communication is one of the main pillars of the applied field of quantum technologies [1], which deals with information-processing tasks that rely on individual and entangled quantum systems. Quantum communication includes many applications, such as quantum cryptography [2,3], quantum bit commitment [4], and quantum secret sharing [5]. Although traditionally many experiments have been performed while resorting to polarization-encoded quantum states [6,7], time-bin-based phase-coding quantum cryptography has always been regarded as the optimal choice for optical fiber communication links due to strong robustness toward environmental disturbances [8–18]. The phase-coding quantum cryptography protocol was initially discussed considering the relative phase between two different single-photon spatial modes defining a long Mach-Zehnder interferometer [8,9]. The main limitation of this original scheme was that the interferometer length needed to be as long as the physical separation between the communicating parties (Alice and Bob), and was thus subjected to strong environmental phase disturbances. More recently, the technology to stabilize long Mach-Zehnder

interferometers supporting the propagation of single photons with short coherence length has become available [19–21], but it nevertheless adds to the experimental complexity.

The time-bin-based configuration was proposed to solve this issue [8,9]. It trades the long single Mach-Zehnder interferometer of the previous scheme with two short unbalanced Mach-Zehnder interferometers (UMZIs), one located at Alice and the other within Bob’s station. Both interferometers are connected with a single optical fiber comprising the communication channel linking Alice and Bob. The key point is that the two long parallel paths of the original phase-encoding scheme are traded for two temporally separate time bins that travel through the same path. This guarantees intrinsic phase stability, since any phase disturbance needs to occur on a timescale shorter than the separation between the two time bins. Only the short UMZIs need to be stabilized, a task considerably easier than actively compensating phase drifts on a long interferometer. The trade-off is an intrinsic loss of 50% at the detection stage due to a postselection of noninterfering time bins. Even more dramatic, this intrinsic loss grows with the dimension  $d$  of the encoded system as  $(d - 1)/d$ , having a larger impact on high-dimensional time-bin quantum communication systems [22]. Despite this, a time bin has been extremely popular since it is much more practical to stabilize two short interferometers instead of a very long one [9].

In this work, we use modern space-division-multiplexing (SDM) fiber-optics technology [23,24] to solve the issue

\* guilherme.b.xavier@liu.se

Published by the American Physical Society under the terms of the Creative Commons Attribution 4.0 International license. Further distribution of this work must maintain attribution to the author(s) and the published article’s title, journal citation, and DOI.

of the irreversible loss at the detection stage of the time-bin scheme, thus providing a pathway toward efficient fiber-based phase-coding quantum communication. Specifically, in our scheme we use a commercial SDM fiber that supports a few linearly polarized (LP) spatial modes, the so-called few-mode fiber (FMF). Similarly to the time-bin configuration, our scheme is based on a single (few-mode) fiber interconnecting two local interferometers for state generation and detection. These states are encoded as a superposition of the LP optical modes supported by the FMF. The key component that allows this implementation is the mode-selective photonic lantern, which takes  $N$  input single-mode fibers, and maps each one-to-one to  $N$  linearly polarized modes of the FMF [25]. As there is no difference in time between the different interferometers' paths, no temporal postselection is needed, and thus there is no irreversible loss in the detection stage. Last, we highlight that our scheme allows the generation and measurement of light modes carrying orbital angular momentum (OAM) in an all-fiber platform, thus dispensing with complex mode multiplexers and sorters based on bulk optics [26–31]. The all-in-fiber generation of OAM light modes is not only useful for classical and quantum communication: the compactness that can be achieved for our OAM source and detection modules can certainly find applications in biophysics [32–34], metrology [35], and astronomy [36], for instance.

## II. EXPERIMENT

In the original phase-encoded scheme, Alice has a single-photon source producing time-localized single photons, whose output is split into two paths through a 50:50 bidirectional fiber coupler. A phase modulator  $\phi_A$  is placed in one of the arms, thus producing quantum states given by  $|\psi\rangle = (1/\sqrt{2})(|0\rangle + e^{i\phi_A}|1\rangle)$ , where  $|0\rangle$  and  $|1\rangle$  correspond to the upper-path and lower-path modes, respectively [Fig. 1(a)]. Both paths are connected to Bob, who also has another phase modulator ( $\phi_B$ ) allowing him to choose between the two required measurement bases. The measurement procedure is concluded with both paths superposed on another 50:50 fiber coupler, followed by a single-photon detector placed in each outcome mode. In this case, the single-photon detection probability at detector 1 (detector 2) is proportional to  $\cos^2(\phi_A - \phi_B)$  [ $\sin^2(\phi_A - \phi_B)$ ], which is a requirement for quantum key distribution, for instance [9].

In the time-bin modification [Fig. 1(b)] Alice first splits an attenuated optical pulse over an *early* (*e*) and a *late* (*l*) time bin with an UMZI, where the imbalance must be greater than the pulse length. Phase modulator  $\phi_A$  is placed inside the interferometer encoding the state  $|\psi\rangle = (1/\sqrt{2})(|e\rangle + e^{i\phi_A}|l\rangle)$ , which propagates toward Bob through an optical fiber. Bob possesses an identical UMZI with phase modulator  $\phi_B$  placed in the

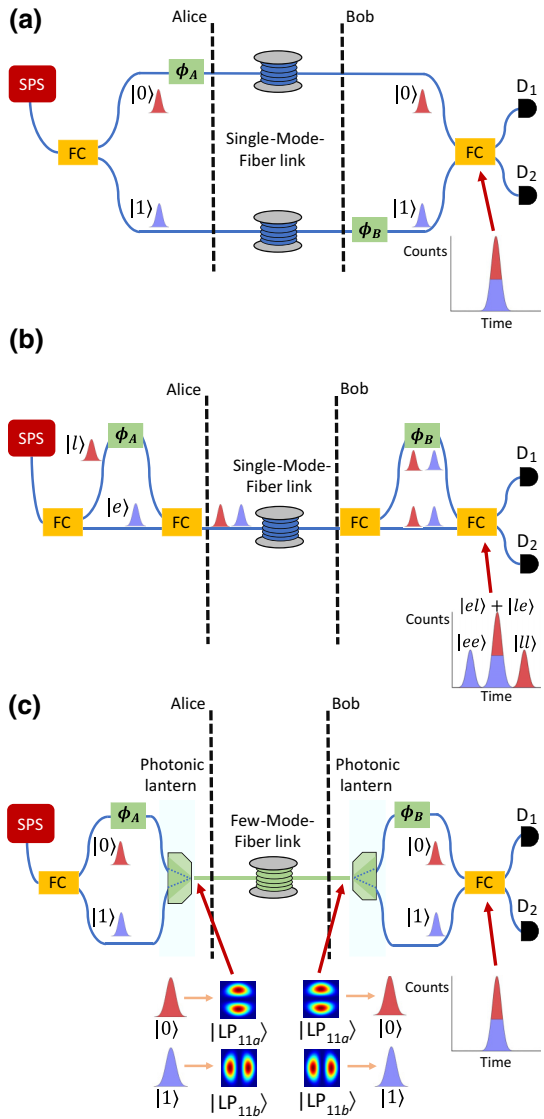


FIG. 1. Phase-coding quantum cryptography. (a) Original scheme based on a long Mach-Zehnder interferometer that must be phase stabilized. Phase modulators are used to prepare and measure the required states. The inset shows that photons transmitted through paths  $|0\rangle$  and  $|1\rangle$  will arrive in the same detection time window. (b) Typical time-bin-based scheme, relying on a single fiber interconnecting two asymmetrical short interferometers (easier to stabilize). Temporal postselection is required. Photons will arrive in three different time bins (see the inset). To extract a secret key, the ones arriving too early or too late must be discarded, thus drastically reducing the communication rate by 50%. (c) Our setup resorting to few-mode-fiber technology. It borrows concepts of the robust time-bin configuration: two short interferometers interconnected through a single (few-mode) fiber. Photons traveling through paths  $|0\rangle$  and  $|1\rangle$  are mapped to orthogonal optical modes supported by the fiber using a photonic lantern, and are demultiplexed in an inverse fashion by another lantern. Since the local interferometers are now symmetrical, these photons will again arrive in the same time bin and no temporal postselection is needed. D, detector; FC, fiber coupler; SPS, single-photon source.

long arm, which is also used to choose his measurement projection. At the outputs of Bob's UMZI, a temporal post-selection procedure is used to detect only photons that took the  $|e\rangle|l\rangle$  path combination or the  $|l\rangle|e\rangle$  path combination. These instances are indistinguishable in principle, and thus display a sinusoidal interference pattern that depends on  $\phi_A - \phi_B$ , which is the same as in the original scheme [Fig. 1(a)]. The other two possibilities that the photons may take ( $|e\rangle|e\rangle$  and  $|l\rangle|l\rangle$ ) are distinguishable, do not interfere, and are thus discarded with temporal postselection [Fig. 1(b), inset]. This represents a loss by a factor of 2 at the detector stage, which is the trade-off when only one fiber is used to connect the communicating parties.

In our experimental demonstration [Fig. 1(c)], the single-photon source consists of a continuous-wave distributed-feedback telecom semiconductor laser (Exfo OS-DFB) operating at 1546 nm. The signal is split into two paths ( $|0\rangle$  and  $|1\rangle$ ) using a 50:50 fiber coupler at Alice's station. A variable optical attenuator placed before the fiber coupler is used to change the power intensity to the single-photon level. A lithium niobate pigtailed telecom phase modulator (Thorlabs LN65S-FC) is placed in one path ( $\phi_A$ ). The phase modulator is driven by an electrical signal from a function generator. The two paths are then connected to a commercial mode-selective photonic lantern (Phoenix Photonics 3PLS-GI-15). This allows multiplexing of information into the spatial modes supported by a FMF through the implementation of the following mode mapping:  $|1\rangle \rightarrow |LP_{11a}\rangle$ ;  $|2\rangle \rightarrow |LP_{11b}\rangle$ . Polarization controllers, not shown for simplicity, are placed in each path  $|0\rangle$  and  $|1\rangle$  to ensure the polarization state of each input mode is the same. We also use a variable attenuator in tandem with a 90:10 fiber coupler before each input to the photonic lantern to ensure each single-mode input has the same optical intensity, thus generating the intended state superpositions.

The FMF link following the lantern consists of either a direct back-to-back connection with only a 10-m-long-FMF manual polarization controller (MPC), or an added spool of FMF with a length of 500 m, with a measured total loss of 1.2 dB, including two homemade fiber connectors. The MPC is used to optimize mode demultiplexing at Bob's lantern. The FMFs used in this experiment are commercially available graded-index telecom fiber (OFS 80730), with a loss coefficient of less than 0.22 dB/km as specified by the manufacturer. The detection stage consists of another photonic lantern that is now used as a demultiplexer, where the inverse mapping is performed. The lantern outputs are the single-mode path states  $|0\rangle$  and  $|1\rangle$ , which are then recombined on another 50:50 fiber coupler. The measurement basis implemented is defined by a second phase modulator ( $\phi_B$ ). Standard MPCs in each arm are also used to align the photon polarization state such that in the final interferometer there is no path information available [37,38], which would compromise the visibility of the

observed interference. Following the final beam splitter, we place (In,Ga)As single-photon-counting modules (IdQ id210) operating with a gate width of 2.5 ns, an internal trigger rate of 1 MHz, overall detection efficiency of 10%, and a dark count probability per gate of  $2.4 \times 10^{-6}$ . An in-fiber polarizer is placed before each detector. Overall, we obtain extinction rates of  $-14.6$  and  $-16.2$  dB when measuring the outputs  $|1\rangle$  and  $|2\rangle$ , respectively, for the opposing inputs ( $|2\rangle$  and  $|1\rangle$ ). The insertion loss given by our commercial lanterns is 6.5 dB.

### III. RESULTS

We focus on the generation of the states that are used for phase-encoding BB84 quantum key distribution [9]. These are based on sets of orthogonal states divided between two mutually unbiased bases [39]. In our case, these states are based on coherent superpositions of LP<sub>11</sub> modes:

$$|LP_{\pm}\rangle = \frac{1}{\sqrt{2}}(|LP_{11a}\rangle \pm |LP_{11b}\rangle), \quad (1)$$

$$|OAM_{\pm}\rangle = \frac{1}{\sqrt{2}}(|LP_{11a}\rangle \pm i|LP_{11b}\rangle). \quad (2)$$

The states  $|OAM_{\pm}\rangle$  are associated with the well-known Laguerre-Gaussian beams carrying OAM [40]. Figure 2(a) shows the theoretical transverse intensity profiles of the  $|LP_{11a}\rangle$  and  $|LP_{11b}\rangle$  modes as well as experimental results in the back-to-back case and after 500 m of propagation, obtained with a linear polarizer and an infrared CCD camera placed after the FMF link. We also measure the intensity profiles associated with the states  $|LP_{\pm}\rangle$  and  $|OAM_{\pm}\rangle$ ,

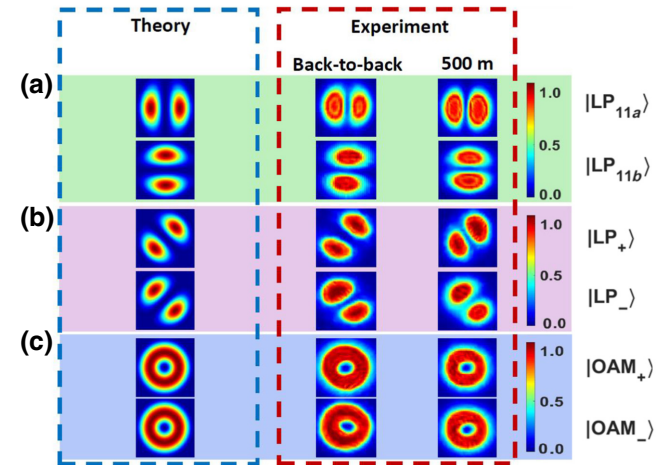


FIG. 2. Spatial intensity profiles of the output of the FMF as measured by an (In,Ga)As CCD camera. (a) Theoretical spatial profiles of the LP<sub>11a</sub> and LP<sub>11b</sub> modes and experimental results in the back-to-back case and after an extra 500 m of FMF. (b),(c) Theoretical and experimental spatial profiles (back-to-back case and after 500-m of propagation) associated with the  $|LP_{\pm}\rangle$  and  $|OAM_{\pm}\rangle$  states, respectively.

which are shown in Figs. 2(b) and 2(c), respectively. Here, each profile is prepared by setting the appropriate phase  $\phi_A = \{0, \pi, \pi/2, 3\pi/2\}$  through a slow driving signal (0.2 Hz) applied to the phase modulator, thus sequentially preparing them. The driving voltage of the phase modulator is calibrated beforehand. To obtain the intensity profiles of the  $|LP_{11a}\rangle$  and  $|LP_{11b}\rangle$  modes, each input arm is individually blocked. For all these measurements, we work with the source in the classical regime, bypassing the variable optical attenuator. These initial results show that the photonic lantern can be used to prepare the coherent quantum superpositions of the spatial states  $|LP_{11a}\rangle$  and  $|LP_{11b}\rangle$ , and also show that these superpositions suffer little degradation following propagation after an extra 500 m, indicating longer distances may be feasible with the current setup.

To demonstrate the feasibility of quantum communication protocols [2,3] in our setup, we remove the CCD camera, reconnect the variable optical attenuator, and connect the output of the FMF to Bob's station as shown in Fig. 1(c). The required states  $|LP_{\pm}\rangle$  and  $|OAM_{\pm}\rangle$  are again prepared by us driving  $\phi_A$  sequentially. The variable attenuator is set to create a weak coherent state with an average mean photon number of  $\mu = 0.4$  per gate width at Alice's output. Therefore, the contribution of multiphoton events is negligible in our experiment. We acquire the detection

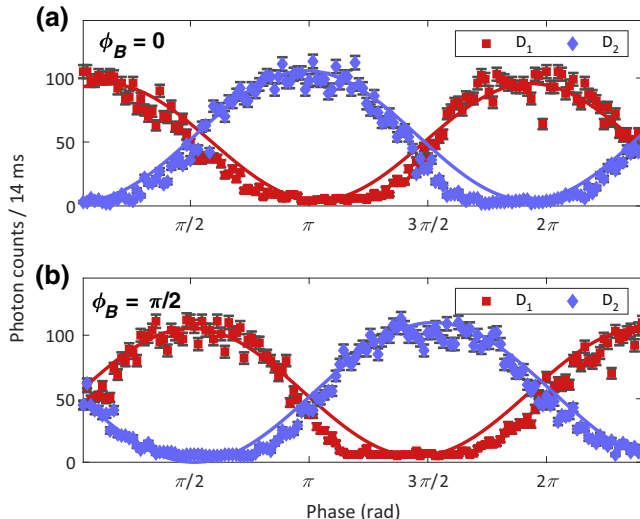


FIG. 3. Single-photon interference curves after 500 m of propagation over the few-mode fiber. The relative phase ( $\phi_A$ ) is modulated with a slow-driving triangular signal. (a) Interference curves recorded while the detection stage is set for measuring at the first mutually unbiased base defined by  $\phi_B = 0$ . (b) Interference curves recorded while the detection stage is set for measuring at the second mutually unbiased base defined by  $\phi_B = \pi/2$ . The standard deviation is calculated assuming Poissonian statistics. The deviation of the experimental data from the theoretical fit is due to the residual phase drift present acting on Alice and Bob's local interferometers, which are not actively phase stabilized. D, detector.

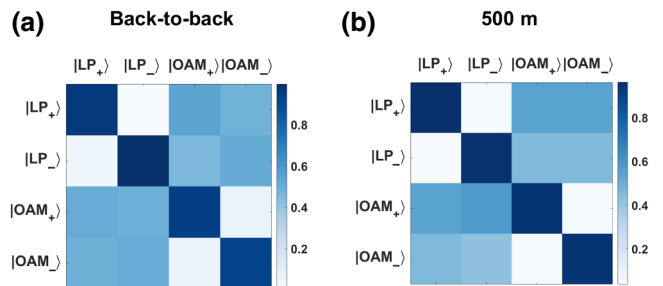


FIG. 4. Probabilities associated with the states of the BB84 quantum cryptography protocol. The vertical axis shows the states being prepared, while the horizontal axis shows onto which state the projection is made. (a) The probabilities in the back-to-back case and (b) the same probabilities following 500 m of propagation over the FMF. See the main text for details.

counts with a short integration time (14 ms) to visualize the interference pattern without active phase stabilization of the first local interferometer. The single-photon interference patterns obtained after 500 m of propagation over the FMF are shown in Fig. 3. Figure 3(a) shows the case corresponding to the detection at the first mutually unbiased basis defined by  $\phi_B = 0$ . In Fig. 3(b), we show the single-photon interference curves obtained with the detection apparatus operating at the second mutually unbiased basis defined by  $\phi_B = \pi/2$ .

From the data points displayed in Fig. 3, we calculate the probabilities of the projection onto state  $i$  given that  $j$  was sent, where  $i, j = \{|LP_+\rangle, |LP_-\rangle, |OAM_+\rangle, |OAM_-\rangle\}$ . The results for the transmitted versus the projected states are plotted in Fig. 4 for both the back-to-back case and the 500 m case. The average probability for the main diagonal (corresponding to the cases where the same state is being transmitted and projected onto) is  $0.955 \pm 0.022$  and  $0.951 \pm 0.024$  for 0 and 500 m, respectively. This points to a lower bound in the error rate for quantum key distribution using this setup and using the BB84 protocol of less than 5% at 500 m, showing the feasibility of this scheme. Out of that number, 0.016% is due to dark counts of the detector. Also, as expected in the BB84 protocol, the probability when performing measurements in the nonmatching bases is around 50%. Furthermore, by considering a simple attenuation model in the single-photon interference curves, we calculate that an extra 3.85-dB loss (corresponding to 17.5 km of FMF) is needed to bring the quantum-key-distribution error rate to 11%, a higher bound where usually no secret key can be generated.

#### IV. CONCLUSION

We propose and experimentally demonstrate a phase-encoded quantum communication system based on few-mode fibers that removes the irreversible detection loss that is present in all time-bin quantum communication systems. While it would be possible to use the polarization

degree of freedom to implement this idea (i.e., sending orthogonal polarization states in the same fiber), it would not allow an expansion to higher dimensions. Our scheme, on the other hand, can be further upgraded to higher dimensions by using few-mode fibers [41], lanterns [42], and beam splitters [43], supporting more modes, while still not presenting extra intrinsic detection losses, thus solving this fundamental issue regarding high-dimensional time-bin encoding (more details are given in the Appendix). Furthermore, our proposal becomes even more effective in a  $d$ -dimensional space, due to the increase of the loss with  $(d - 1)/d$ . Recently multicore fibers have been successfully used to transport spatially encoded quantum states [44], but they still suffer from a slow phase drift because each mode takes a separate core in the fiber [45]. FMFs, on the other hand, show no such drift, since the modes propagate in the same core (see the Appendix), showing they may be ideal for this application. Other recently demonstrated lanterns have had losses as low as 0.7 dB for a six-mode lantern [46], with recent simulations pointing out that lanterns of much lower losses (0.1 dB) could be achieved [40], further demonstrating the attractiveness of our scheme as a path in the future use of time-bin encoding for quantum communication. For the specific case of qubit-based time-bin quantum communication systems, if one uses improved lanterns with 0.7-dB losses, then there is an increase of approximately 70% in the overall detection efficiency compared with a standard time-bin system, with the gain increasing if higher-dimensional systems are used. Finally, although we use BB84 as an illustrative example of the possibilities of our setup for quantum information, other applications can benefit directly from the removed detection losses, such as high-dimensional quantum cryptography [22] and quantum random access codes [47].

Another major achievement that further shows that SDM technology can provide more significant benefits to quantum information [23] is the use of photonic lanterns to generate and decode OAM spatial states completely in-fiber, which also has important applications in optical communications [48]. Finally, recent developments in integrated photonic circuits [49] could completely replace Alice and Bob's optical setups with integrated chips, greatly increasing compactness and robustness, and thus dismissing the need for active phase stabilization. We therefore envisage these results will have a significant and imminent impact in areas such as long-distance quantum communication and high-dimensional quantum information and as a tool to further increase the capacity of classical communication networks.

## ACKNOWLEDGMENTS

We acknowledge Ceniiit Linköping University, the Swedish Research Council (Grant No. 2017-04470),

QuantERA SECRET (Grant No. 2019-00392), and the Knut and Alice Wallenberg Foundation through the Wallenberg Center for Quantum Technology for financial support. G.L. was supported by Fondo Nacional de Desarrollo Científico y Tecnológico (Grant No. 1200859) and the ANID Millennium Science Initiative program (Grant No. ICN17\_012).

## APPENDIX: EXPANSION TO HIGHER DIMENSIONS

Our scheme is directly scalable by using SDM components that support a higher number of modes: lanterns [42], few-mode fibers [41], and multiport beam splitters [43]. Furthermore, our scheme becomes even more beneficial at higher dimensions, due to the greatly increasing loss with  $d$  for the time-bin configuration. The proposal is shown in Fig. 5, where we split the output of the single-photon source into a total of  $d$  paths using a multiport beam splitter. Each path has a different phase modulator  $\phi_n$ , with  $n$  ranging from 0 to  $d - 1$ , allowing the preparation of the high-dimensional path state  $|\Psi\rangle = 1/\sqrt{d} \sum_{n=0}^{d-1} e^{i\phi_n} |n\rangle$ , where  $|n\rangle$  represents the  $n$ th path and  $1/\sqrt{d}$  is a normalization factor. Then each path is connected to a  $d$ -mode photonic lantern to excite the corresponding LP mode in a  $d$ -mode FMF. Finally, another  $d$ -mode lantern is used to demultiplex the LP modes into the corresponding  $d$  paths, which contain the phase modulators  $\phi'_n$  to choose the state projection. Finally, an  $d \times d$  multiport beam splitter is used to superpose the different paths, and the  $d$  outputs are connected to single-photon detectors. Note that no temporal postselection is needed, as in the two-dimensional case.

### 1. Phase stability of phase-encoded states over a FMF

As discussed in the main text, phase encoding is not usually used in the original Mach-Zehnder configuration since the channel is not held stable long enough for a key exchange to occur, due to fast phase instabilities.

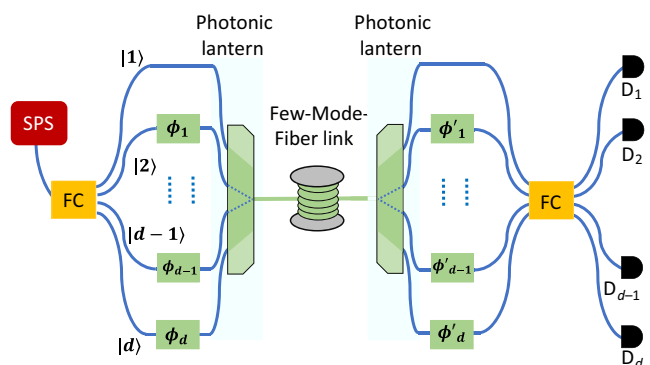


FIG. 5. Qudit-based quantum communication scheme using phase encoding with few-mode fibers. D, detector; FC, fiber coupler; SPS, single-photon source.

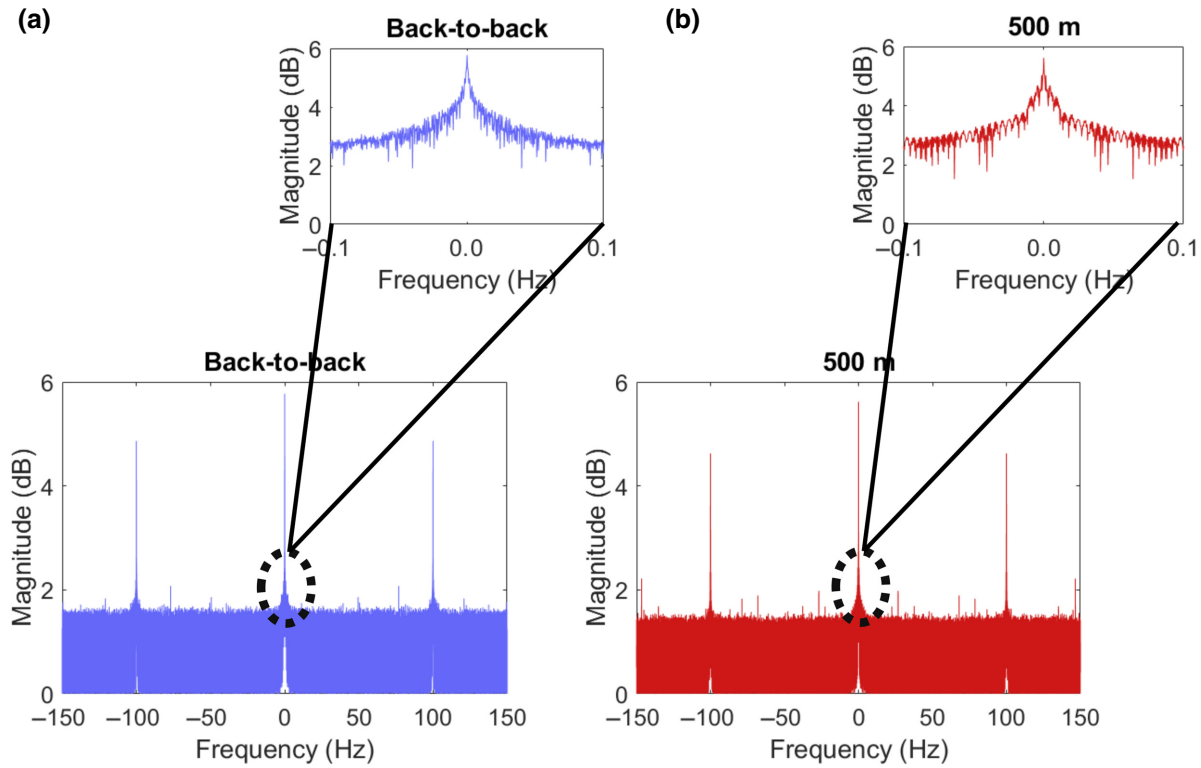


FIG. 6. Fourier spectra of 50 min-long measurements of the interferometer output, when the input state is continuously modulated with a 100-Hz sinusoidal wave, for both the back-to-back case (a) and after an extra 500 m of FMF (b).

Although multicore fibers show a considerable improvement in this aspect when compared with independent single-mode fibers, they still have a residual drift that requires active phase-drift compensation [44,45]. FMFs, on the other hand, have the advantage that the individual spatial modes travel through the same core, which is more intrinsically stable than independent cores in the same cladding.

To demonstrate the stability, we adjust the attenuator at the output of the laser source to work with classical optical power levels. We then continuously modulate the input state through the phase modulator  $\phi_A$  with a 100-Hz sinusoidal wave for 50 min, both in the back-to-back case (10 m) and with the 500-m-long spool connected. The output from the final beam splitter in Fig. 1(c) is measured with a *p-i-n* photodiode. The driving voltage is meant to impose a clear modulation signal creating well-defined interference fringes. The output from the photodiode is recorded with an oscilloscope. Figures 6(a) and 6(b) show the Fourier transforms of the recorded 50-min time signal for the back-to-back case and the 500-m case, respectively. The inset shows enlargements around the center peak at 0 Hz. The environmental phase drift acting on an interferometric setup in the laboratory is typically characterized by low-frequency components. In our case, there is substantial phase drift acting over Alice and Bob's

components, which consist of parallel paths (single-mode fibers). From comparison of both spectra (back-to-back case and 500-m case), it is clear there is no significant difference in the low-frequency region, or even across a broader frequency range. This result shows that adding an extra 500 m of FMF does not increase the environmental phase drift, which leads to the possibility that FMFs can be used as a platform for phase-encoded states over longer distances.

To further corroborate the benefits of using a FMF in this regard, we perform a brief comparison based on two multicore-fiber interferometers previously used in other experiments. In Ref. [44], it was demonstrated that tens of minutes were needed for the environmental phase drift to cause a complete inversion in the detected state in a 300-m-long multicore-fiber interferometer. In Ref. [45], it can be seen that an equivalent measurement on a 2-km-long multicore-fiber interferometer takes on the order of tens of seconds. While it is difficult to make a precise measurement on the difference, because the two experiments were done in different laboratories, both experiments still showed a clear difference when the distance is increased from 300 m to 2 km in multicore-fiber interferometers. In our case, as we can observe no appreciable difference when moving from the back-to-back case to the 500-m case, this further shows the benefits of using FMFs in this regard.

- [1] A. Acín, I. Bloch, H. Buhrman, T. Calarco, C. Eichler, J. Eisert, D. Esteve, N. Gisin, S. J. Glaser, F. Jelezko, *et al.*, The quantum technologies roadmap: A European community view, *New J. Phys.* **20**, 080201 (2018).
- [2] F. Xu, X. Ma, Q. Zhang, H.-K. Lo, and J.-W. Pan, Secure quantum key distribution with realistic devices, *Rev. Mod. Phys.* **92**, 025002 (2020).
- [3] S. Pirandola, U. L. Andersen, L. Banchi, M. Berta, D. Bunandar, R. Colbeck, D. Englund, T. Gehring, C. Lupo, C. Ottaviani, *et al.*, Advances in quantum cryptography, *Adv. Opt. Photonics* **12**, 1012 (2020).
- [4] T. Lunghi, J. Kaniewski, F. Bussières, R. Houlmann, M. Tomamichel, A. Kent, N. Gisin, S. Wehner, and H. Zbinden, Experimental Bit Commitment Based on Quantum Communication and Special Relativity, *Phys. Rev. Lett.* **111**, 180504 (2013).
- [5] J. Pinnell, I. Nape, M. de Oliveira, N. Tabebordbar, and A. Forbes, Experimental demonstration of 11-dimensional 10-party quantum secret sharing, *Laser Photonics Rev.* **14**, 2000012 (2020).
- [6] G. B. Xavier, N. Walenta, G. Vilela de Faria, G. P. Temporão, N. Gisin, H. Zbinden, and J. P. von der Weid, Experimental polarisation encoded quantum key distribution over optical fibres with real-time continuous birefringence compensation, *New J. Phys.* **11**, 045015 (2009).
- [7] F. Grünenfelder, A. Boaron, D. Rusca, A. Martin, and H. Zbinden, Simple and high-speed polarisation-based QKD, *Appl. Phys. Lett.* **112**, 051108 (2018).
- [8] C. H. Bennett, Quantum Cryptography Using Any Two Nonorthogonal States, *Phys. Rev. Lett.* **68**, 3121 (1992).
- [9] N. Gisin, G. Ribordy, W. Tittel, and H. Zbinden, Quantum cryptography, *Rev. Mod. Phys.* **74**, 145 (2002).
- [10] P. Townsend, J. G. Rarity, and P. R. Tapster, Single photon interference in a 10 km long optical fibre interferometer, *Electron. Lett.* **29**, 634 (1993).
- [11] C. Gobby, Z. L. Yuan, and A. J. Shields, Quantum key distribution over 122 km of standard telecom fibre, *Appl. Phys. Lett.* **84**, 3762 (2004).
- [12] Q. Wang, W. Chen, G. Xavier, M. Swillo, T. Zhang, S. Sauge, M. Tengner, Z.-F. Han, G.-C. Guo, and A. Karlsson, Experimental Decoy-State Quantum Key Distribution with a Sub-Poissonian Heralded Single-Photon Source, *Phys. Rev. Lett.* **100**, 090501 (2008).
- [13] Z. L. Yuan, A. R. Dixon, J. F. Dynes, A. W. Sharpe, and A. J. Shields, Gigahertz quantum key distribution with InGaAs avalanche photodiodes, *Appl. Phys. Lett.* **92**, 201104 (2008).
- [14] S. Wang, W. Chen, J.-F. Guo, Z.-Q. Yin, H.-W. Li, Z. Zhou, G.-C. Guo, and Z.-F. Han, 2 GHz clock quantum key distribution over 260 km of standard telecom fibre, *Opt. Lett.* **37**, 1008 (2012).
- [15] A. Rubenok, J. A. Slater, P. Chan, I. Lucio-Martinez, and W. Tittel, Real-World Two-Photon Interference and Proof-Of-Principle Quantum Key Distribution Immune to Detector Attacks, *Phys. Rev. Lett.* **111**, 130501 (2013).
- [16] Y. Liu, T.-Y. Chen, L.-J. Wang, H. Liang, G.-L. Shentu, J. Wang, K. Cui, H.-L. Yin, N.-L. Liu, L. Li, *et al.*, Experimental Measurement-Device-Independent Quantum Key Distribution, *Phys. Rev. Lett.* **111**, 130502 (2013).
- [17] N. T. Islam, C. C. W. Lim, C. Cahall, J. Kim, and D. J. Gauthier, Provably secure and high-rate quantum key distribution with time-bin qudits, *Sci. Adv.* **3**, e1701491 (2017).
- [18] A. Boaron, B. Korzh, R. Houlmann, G. Bosco, D. Rusca, S. Gray, M.-J. Li, D. Nolan, A. Martin, and H. Zbinden, Simple 2.5 GHz time-bin quantum key distribution, *Appl. Phys. Lett.* **112**, 171108 (2018).
- [19] G. B. Xavier, G. P. Temporão, and J. P. von der Weid, Employing long fibre-optical Mach-Zehnder interferometers for quantum cryptography with orthogonal states, *Electron. Lett.* **48**, 775 (2012).
- [20] Á. Cuevas, G. Carvacho, G. Saavedra, J. Cariñé, W. A. T. Nogueira, M. Figueroa, A. Cabello, P. Mataloni, G. Lima, and G. B. Xavier, Long-distance distribution of genuine energy-time entanglement, *Nat. Commun.* **4**, 2871 (2013).
- [21] G. Carvacho, J. Cariñé, G. Saavedra, Á. Cuevas, J. Fuenzalida, F. Toledo, M. Figueroa, A. Cabello, J.-Å. Larsson, P. Mataloni, *et al.*, Postselection-Loophole-Free Bell Test Over an Installed Optical Fibre Network, *Phys. Rev. Lett.* **115**, 030503 (2015).
- [22] N. T. Islam, C. Cahall, A. Aragoneses, A. Lezama, J. Kim, and D. J. Gauthier, Robust and Stable Delay Interferometers with Application to  $d$ -Dimensional Time-Frequency Quantum Key Distribution, *Phys. Rev. Appl.* **7**, 044010 (2017).
- [23] G. B. Xavier and G. Lima, Quantum information processing with space-division multiplexing optical fibres, *Commun. Phys.* **3**, 9 (2020).
- [24] D. J. Richardson, J. M. Fini, and L. E. Nelson, Space-division multiplexing in optical fibres, *Nat. Photonics* **7**, 354 (2013).
- [25] T. A. Birks, I. Gris-Sánchez, S. Yerolatsis, S. G. Leon-Saval, and R. R. Thomson, The photonic lantern, *Adv. Opt. Photonics* **7**, 107 (2015).
- [26] G. C. G. Berkhout, M. P. J. Lavery, J. Courtial, M. W. Beijersbergen, and M. J. Padgett, Efficient Sorting of Orbital Angular Momentum States of Light, *Phys. Rev. Lett.* **105**, 153601 (2010).
- [27] M. P. J. Lavery, D. J. Robertson, G. C. G. Berkhout, G. D. Love, M. J. Padgett, and J. Courtial, Refractive elements for the measurement of the orbital angular momentum of a single photon, *Opt. Express* **20**, 2110 (2012).
- [28] H. Huang, G. Milione, M. P. J. Lavery, G. Xie, Y. Ren, Y. Cao, N. Ahmed, T. A. Nguyen, D. A. Nolan, M.-J. Li, *et al.*, Mode division multiplexing using an orbital angular momentum mode sorter and MIMO-DSP over a graded-index few-mode optical fibre, *Sci. Rep.* **5**, 14931 (2015).
- [29] Y. Wen, I. Chremmos, Y. Chen, G. Zhu, J. Zhang, J. Zhu, Y. Zhang, J. Liu, and S. Yu, Compact and high-performance vortex mode sorter for multi-dimensional multiplexed fibre communication systems, *Optica* **7**, 254 (2020).
- [30] Huan Cao, She-Cheng Gao, Chao Zhang, Jian Wang, De-Yong He, Bi-Heng Liu, Zheng-Wei Zhou, Yu-Jie Chen, Zhao-Hui Li, Si-Yuan Yu, *et al.*, Distribution of high-dimensional orbital angular momentum entanglement over a 1 km few-mode fiber, *Optica* **7**, 232 (2020).

- [31] J. Liu, I. Nape, Q. Wang, A. Vallés, J. Wang, and A. Forbes, Multidimensional entanglement transport through single-mode fiber, *Sci. Adv.* **6**, eaay0837 (2020).
- [32] M. J. Padgett and R. Bowman, Tweezers with a twist, *Nat. Photonics* **5**, 343 (2011).
- [33] D. G. Grier, A revolution in optical manipulation, *Nature* **424**, 810 (2003).
- [34] S. Franke-Arnold, L. Allen, and M. J. Padgett, Advances in optical angular momentum, *Laser Photonics Rev.* **2**, 299 (2008).
- [35] V. D'Ambrosio, N. Spagnolo, L. Del Re, S. Slussarenko, Y. Li, L. C. Kwek, L. Marrucci, S. P. Walborn, L. Aolita, and F. Sciarrino, Photonic polarization gears for ultra-sensitive angular measurements, *Nat. Commun.* **4**, 2432 (2013).
- [36] F. Tamburini, B. Thidé, G. Molina-Terriza, and G. Anzolin, Twisting of light around rotating black holes, *Nat. Phys.* **7**, 195 (2011).
- [37] S. P. Walborn, M. O. Terra Cunha, S. Pádua, and C. H. Monken, Double-slit quantum eraser, *Phys. Rev. A* **65**, 033818 (2002).
- [38] F. A. T. Ruiz, G. Lima, A. Delgado, S. Pádua, and C. Saavedra, Decoherence in a double-slit quantum eraser, *Phys. Rev. A* **81**, 042104 (2010).
- [39] M. Mafu, A. Dudley, S. Goyal, D. Giovannini, M. McLaren, M. J. Padgett, T. Konrad, F. Petruccione, N. Lütkenhaus, and A. Forbes, Higher-dimensional orbital-angular-momentum-based quantum key distribution with mutually unbiased bases, *Phys. Rev. A* **88**, 032305 (2013).
- [40] Y. Li, Y. Li, L. Feng, C. Yang, W. Li, J. Qiu, X. Hong, Y. Zuo, H. Guo, W. Tong, *et al.*, Mode-selective photonic lanterns for orbital angular momentum mode division multiplexing, *Appl. Sci.* **9**, 2233 (2019).
- [41] P. Sillard, M. Bigot-Astruc, and D. Molin, Few-mode fibres for mode-division-multiplexed systems, *IEEE J. Lightwave Technol.* **32**, 2824 (2014).
- [42] A. M. Velázquez-Benítez, J. E. Antonio-López, J. C. Alvarado-Zacarías, N. K. Fontaine, R. Ryf, H. Chen, J. Hernández-Cordero, P. Sillard, C. Okonkwo, Chigo Okonkwo, *et al.*, Scaling photonic lanterns for space-division multiplexing, *Sci. Rep.* **8**, 8897 (2018).
- [43] J. Cariñé, G. Cañas, P. Skrzypczyk, I. Šupić, N. Guerrero, T. Garcia, L. Pereira, M. A. S. Prosser, G. B. Xavier, A. Delgado, *et al.*, Multi-core fibre integrated multi-port beam splitters for quantum information processing, *Optica* **7**, 542 (2020).
- [44] G. Canás, N. Vera, J. Cariñé, P. González, J. Cardenas, P. W. R. Connolly, A. Przysiezna, E. S. Gómez, M. Figueroa, G. Vallone, *et al.*, High-dimensional decoy-state quantum key distribution over multicore telecommunication fibres, *Phys. Rev. A* **96**, 022317 (2017).
- [45] B. Da Lio, D. Bacco, D. Cozzolino, N. Biagi, T. N. Arge, E. Larsen, K. Rottwitt, Y. Ding, A. Zavatta, and L. K. Oxenløwe, Stable transmission of high-dimensional quantum states over a 2-km multicore fibre, *IEEE J. Sel. Top. Quantum Electron.* **26**, 6400108 (2019).
- [46] A. M. Velázquez-Benítez, J. C. Alvarado-Zacarías, G. Lopez-Galmiche, J. E. Antonio-López, A. Schülgen, D. V. Ras, P. Sillard, C. Okonkwo, and R. Amezcua-Correa, in *Optical Fibre Communication Conference*, OSA Technical Digest (online) (Optical Society of America, Los Angeles, USA, 2015), paper W3B.3.
- [47] A. Tavakoli, A. Hameedi, B. Marques, and M. Bourennane, Quantum Random Access Codes Using Single  $d$ -Level Systems, *Phys. Rev. Lett.* **114**, 170502 (2015).
- [48] N. Bozinovic, Y. Yue, Y. Ren, M. Tur, P. Kristensen, H. Huang, A. E. Willner, and S. Ramachandran, Terabit-scale orbital angular momentum mode division multiplexing in fibres, *Science* **340**, 1545 (2013).
- [49] J. Wang, F. Sciarrino, A. Laing, and M. G. Thompson, Integrated photonic quantum technologies, *Nat. Photonics* **14**, 273 (2020).

*Correction:* The previously published Figure 4 contained incorrect labels and erroneous colors to represent probability values in panel (b) and has been replaced.

*Second Correction:* The copyright license statement was presented incorrectly and has been fixed.